JMEPEG (2010) 19:1298–1305
DOI: 10.1007/s11665-010-9622-4

1059-9495/$19.00

Damage Progression and Stress Redistribution in Notched SiC/SiC Composites

Andrew L. Gyekenyesi and Gregory N. Morscher

(Submitted July 13, 2009; in revised form February 9, 2010)

The stress fields adjacent to machined notch roots were examined during tensile tests of woven SiC/SiC composites using thermoelastic stress analysis. As expected, the stress-concentration factor (SCF) at the notch roots increased with increasing notch lengths. Damage-induced stress-relief was not evident in these composites. In fact, the redistribution of stresses onto isolated fiber tows adjacent to the notch root caused an increase in the apparent SCF. Lastly, the SCF increased with mean stress. This was assumed to occur as a result of opening matrix cracks that are typically closed due to residual compressive stresses in the matrix material at near zero loads.

Keywords ceramic matrix composites (CMCs), damage, notch, stress-concentrations, thermoelastic stress analysis (TSA)

1. Introduction

Woven silicon carbide (SiC) fiber SiC matrix composites are considered to be candidate materials for combustor liners and other components of future turbine engine applications (Ref 1-4). This class of materials possesses good high-temperature creep and rupture properties, and exhibits reasonably good thermal conductivity. However, there are a number of properties and material behaviors that need to be understood prior to full acceptance as applicable structural materials. One topic of concern is related to stress-concentrations (e.g., notches, holes, or attachment points). Stress risers may adversely affect the mechanical behavior of these composites at room and elevated temperatures. A desirable attribute of ceramic matrix composites (CMCs), in general, is their reduced sensitivity to the presence of notches or holes in comparison to monolithic ceramics (Ref 5). CMCs exhibit fiber-bridged matrix cracking above a certain threshold stress. Matrix cracking, in the vicinity of a stress-concentration, enables stress redistribution, thereby reducing the magnitude of the local stress-concentration (Ref 6). Most of the research in this arena has sought to determine the effect of notch or hole size on the ultimate strength properties of CMCs at room temperature. The ultimate strengths of some CMC systems have been shown to be notch insensitive (Ref 7, 8) and others only slightly notch sensitive (Ref 9, 10). Notch strength data have shown SiC/SiC composites to be mildly notch sensitive (Ref 10, 11).

Andrew L. Gyekenyesi, Ohio Aerospace Institute, NASA GRC, 21000 Brookpark Road MS 6-1, Cleveland, OH 44135; and **Gregory N. Morscher**, The Department of Mechanical Engineering, University of Akron, ASEC, Rm 101, Akron, OH 44325. Contact e-mails: Andrew.L.Gyekenyesi@nasa.gov and Gm33@uakron.edu.

It is expected that typical applications for CMCs will have local areas of stress-concentration due to thermal gradients, geometric discontinuities, and/or joining incompatibilities. However, the applied stress for such applications will be considerably lower than the ultimate strength. In addition, CMCs will be expected to survive extended periods of time at elevated temperatures in severe oxidizing environments. Therefore, an understanding of the damage accumulation and the stress-state around stress-concentrators at applied loads well below the ultimate strength is a necessity. Such knowledge is required to complement a data base of notch-dependent ultimate strengths. This study addresses the issue of stress-relief due to inelastic damage mechanisms. Two types of woven SiC fiber reinforced, BN interphase, melt-infiltrated (MI) SiC matrix composites were studied. The composites differ in their fiber reinforcement; one system had Hi-Nicalon™ fibers whereas the other system was composed of the stiffer Sylramic® fiber-type. Room temperature, uniaxial tensile tests were conducted using standard double-edge notch specimens. Surface stress profiles of the notched specimens were obtained by employing the thermoelastic stress analysis (TSA) technique. The TSA images allowed for a relative analysis of the stress-concentration behavior as a function of notch length, damage level, and in situ stress level. It should be noted that this study supplements an earlier research effort (Ref 11) by the authors concerning the notch sensitivity of SiC/SiC composites. For that study, parametric experimentation was utilized in order to define the ultimate tensile strength at room temperature as a function of notch length and specimen width. Modal acoustic emissions and post-test destructive sectioning were used for characterizing the progression of damage.

2. Experimental Procedure

2.1 TSA Theory

TSA is a full-field, noncontacting technique for surface stress mapping of structures. TSA is based on the fact that materials experience a temperature change when compressed or

expanded (i.e., experience a change in volume). If the load causing, the volumetric change is removed and the material returns to its original temperature and shape, the process is deemed reversible. This reversibility is achieved when a material is loaded elastically at a high enough rate so as to eliminate significant conduction of heat. The thermoelastic temperature change, in CMCs for instance, as a result of a typical cyclic load in the nondamaging elastic range is between 0.01 and 0.1 °C (Ref 12).

Lord Kelvin (Ref 13) first quantified an analytical relationship between the change in temperature and the change in stress. The formulation is as follows:

$$\frac{\delta T}{T_o} = \frac{-\alpha \delta I_1}{\rho C_p} \quad \text{(Eq 1)}$$

$$= -K\delta I_1, \quad \text{(Eq 2)}$$

where δT is the cyclic change in temperature; α is the coefficient of linear thermal expansion; T_o is the absolute temperature of the specimen; δI_1 is the cyclic change in the sum of the principal stresses; ρ is the material density; C_p is the specific heat at constant pressure; and K is the thermoelastic constant. Note that the method allows for a two-dimensional stress map of a loaded structure with spatial variations in the stress field showing up as spatial variations in the temperature profile.

2.2 TSA Procedure

The TSA system employed for this study utilizes a liquid nitrogen cooled infrared (IR) camera with a 128×128 focal plane array of detectors to measure the surface temperatures of the cyclically loaded, notched specimens. The system operates by recording a periodic temperature change, as viewed by the IR camera, of a specimen subjected to a cyclic mechanical load. The system is schematically represented in Fig. 1. A reference signal from the load cell is used by the software to allow it to monitor only the true thermoelastic change in temperature and to disregard any noise and environmental effects that do not correlate with the reference signal's primary frequency. This is accomplished by using a lock-in detection method (Ref 14). The lock-in technique filters the thermal response allowing the analysis of only the TSA frequency component that corresponds to the primary frequency of the reference signal. To further improve the TSA signal-to-noise ratio, the IR signal is monitored, accumulated, and averaged over a period of hundreds or thousands of load cycles. When an image is captured, the computer display depicts a dimensionless, digitized value of the average camera signal range corresponding to the cyclic load range for each of the 16384 pixels. For typical structural stress measurements, the dimensionless digital IR values are correlated to a known cyclic stress amplitude (e.g., as measured by a strain gage which represents a finite, local area) and then utilized to map the surface stress amplitudes of the entire structure.

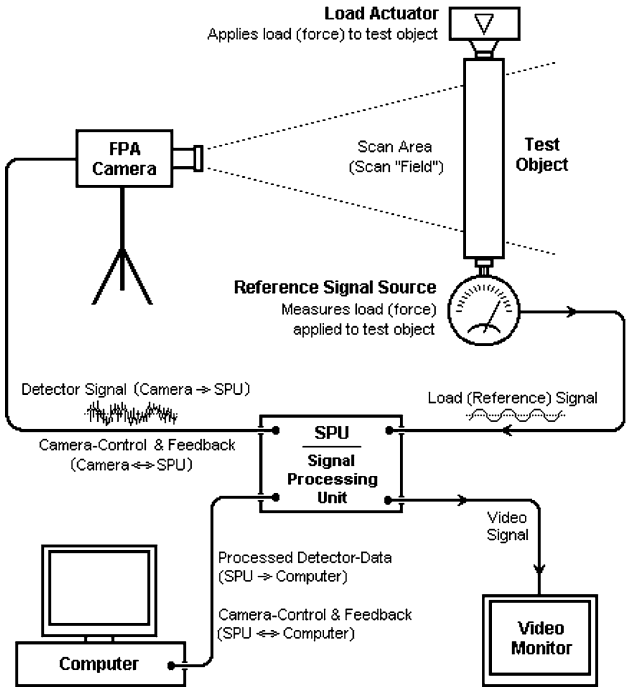

Fig. 1 Schematic diagram of TSA system (DeltaTherm 1000 User's Manual)

During this study, the applied cyclic stress levels used to obtain a TSA response were kept low enough so that no further damage was induced in the CMC specimens (i.e., the current state of damage was maintained). The line scans of the TSA images between the two notches were analyzed and used to compute a relative stress-concentration factor (SCF) (Ref 12). The SCF was calculated using the following relationship:

$$\mathrm{SCF} = \frac{\Delta\sigma_{\mathrm{local}}}{\Delta\sigma_{\mathrm{net}}} = \frac{\Delta T_{\mathrm{local}}}{\Delta T_{\mathrm{farfield}}\left(\frac{A_{\mathrm{farfield}}}{A_{\mathrm{net}}}\right)}, \quad \text{(Eq 3)}$$

where ΔT is the measured temperature range as represented by the dimensionless digital values of the captured TSA image; $\Delta\sigma$ is stress, and A is the cross-sectional area of the specimen. Hence, the SCF is the ratio of the actual measured stress near the notch root, $\Delta\sigma_{\mathrm{local}}$, and the net section stress, $\Delta\sigma_{\mathrm{net}}$, which takes into account the reduced area between the notches $\left[\Delta\sigma_{\mathrm{net}} = \Delta\sigma_{\mathrm{farfield}}\left(\frac{A_{\mathrm{farfield}}}{A_{\mathrm{net}}}\right)\right]$.

The TSA was conducted using the DeltaTherm 1000 system manufactured by Stress Photonics Incorporation. The distance from the camera lens to the specimen was 11.4 cm. This equated to a pixel resolution of approximately 0.25 mm. The following system software settings were utilized during IR data acquisition: Accumulation Time = 4.7 s; Gain = 4; and AC Channel Integration Time constant = 60 s.

2.3 Materials

The composite materials studied consisted of woven Sylramic or Hi-Nicalon fibers with a BN interphase that had a melt-infiltrated SiC matrix. The Sylramic fiber system is designated as SYLMI, and the Hi-Nicalon system is referred to as HNMI. The materials were processed by Honeywell Advanced Composites Inc. (Newark, Delaware) and supplied in the form of panels for each system. In summary, the processing steps were as follows: (1) eight plies of woven (five harness satin) cloth were stacked to form a preform, (2) the preform was chemical vapor infiltrated (CVI) with BN, (3) the BN-coated preform was infiltrated (CVI) with a thin, ~2 μm, thick layer of SiC, (4) the SiC-coated preform was infiltrated with a SiC particle slurry and then infiltrated with liquid silicon to near full

density. For further details related to processing, see Ref 1. Some properties of the composites used in this study are tabulated in Table 1 (Ref 11). Four-notched specimens (two for each fiber-type) were mechanically tested and analyzed using TSA. Test preparation included painting all the specimens with an ultra-flat black paint to improve surface emissivity. The straight-sided specimens were 15 cm long and had two different specimen widths and a variety of notch sizes. Figure 2 shows a schematic representation of a notched specimen.

Table 1 Physical properties of composites (Ref 11)

Composite	Fiber volume fraction, %	Elastic modulus, GPa	Panel density, g/cc
HNMI	33.1	161	2.77
SYLMI	40.7	225	2.83

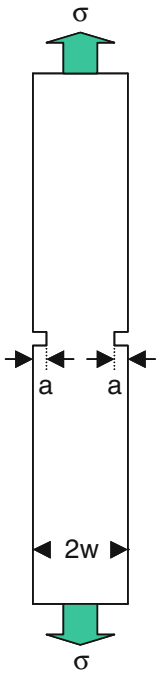

Fig. 2 Schematic of double-edge notch specimen

Table 2 provides details concerning the specimen and notch geometries as well as describing the goals of the experiments for each specimen. A 12.7 cm × 0.4 mm diamond impregnated wafering blade (Buehler, Lake Bluff, IL) was used to cut and extend the notches resulting in a notch radius of approximately 0.2 mm.

2.4 Experimental Procedure

A servo-hydraulic, uniaxial test system with hydraulic actuated grips was utilized for loading the specimens. All tests were conducted using load control. During the TSA captures, a 10-Hz sinusoidal wave form was employed for the loading of the specimen. This frequency was shown to provide consistent adiabatic results for similar notched materials in Ref 6. The uniform phase images captured during this study also supported the assumption of adiabatic conditions. The cyclic stress range was fixed at 35 MPa while the mean stress was maintained at 17.5 MPa, except for specimen 001c. For that particular specimen, the mean stress was varied in order to analyze the notch behavior (i.e., the stress profile adjacent to the notch) as a function of in situ stress during TSA data capture. To induce damage or increase the current damage state, the specimens were mechanically loaded in a repeated load/unload/reload fashion. With each reload, the maximum stress level was progressively increased. The increasing stress rate was 0.69 MPa/s, while the decreasing stress rate was 2.1 MPa/s during the damage-inducing tests. The maximum stress values (i.e., the reversal points) for each damage-inducing load/unload test are summarized in Table 2.

3. Results and Discussion

3.1 TSA Results

Figure 3 shows the TSA results for the HNMI composite concerning the notch length dependence. Included in the figure are the TSA images and horizontal line scans between notch tips as a function of increasing notch length. The line scan values were based on Eq 3 with ΔT_{local} utilizing the dimensionless temperature data from the raw line scans and $\Delta T_{\text{farfield}}$ using an average of the dimensionless temperature data in the rectangular boxes near the top of each of the TSA images. Similar tests were conducted using the SYLMI composite, and the results are presented in Fig. 4. It was observed that the peak

Table 2 Test details for specimens

Specimen ID	Composite	Specimen width, 2*w*, mm	Total notch lengths, 2*a*, mm	Max stress levels (a), MPa	Test goals: Notch stress dependence on…
N001a	HNMI	15	4	69, 103, 138, 207, 241	Damage
001c	HNMI	25	2, 4, 8 (b)	138, 207, 241	Notch length, Damage (b), In situ (mean) stress of 17.5, 69, 138, 207 MPa
N015a	SYLMI	15	4	69, 103, 138, 207	Damage
015c	SYLMI	25	2, 4, 8	None	Notch length

(a) Maximum stress levels for load reversals during load/unload/reload damage progression tests (based on net area)
(b) Damage was not induced until the final notch size was cut

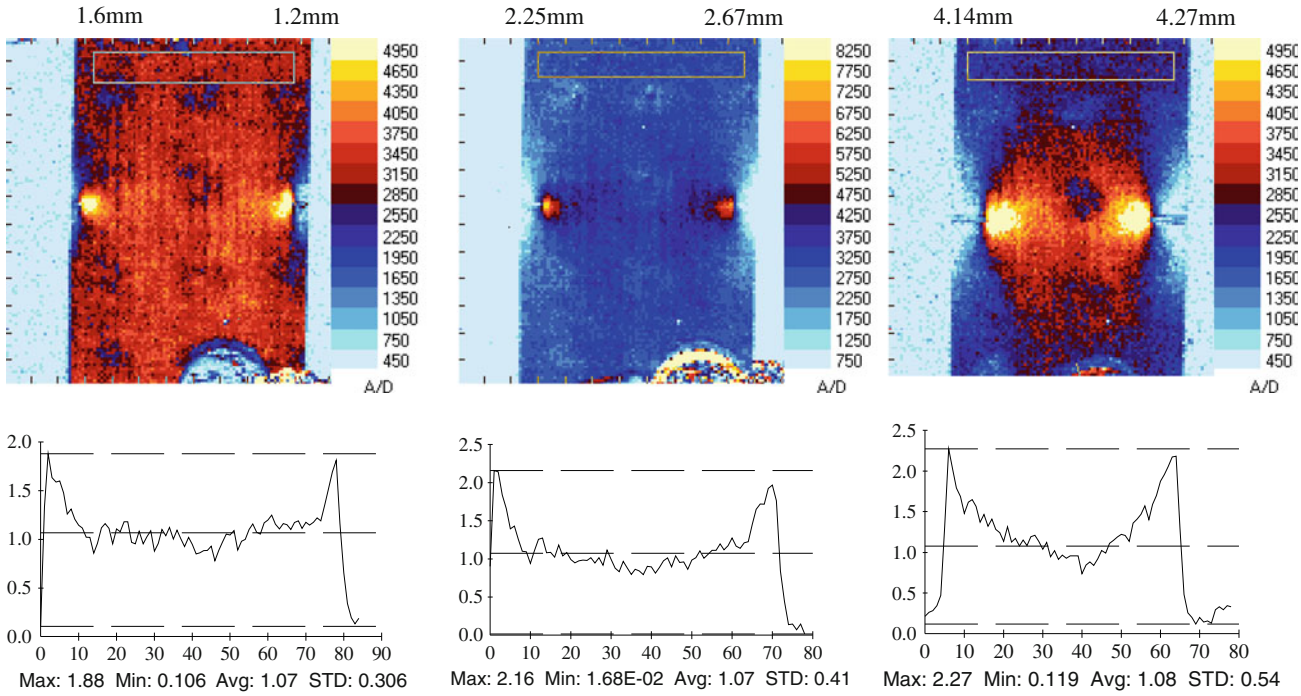

Fig. 3 TSA images and SCFs for HNMI (specimen 001c) as a function of increasing notch lengths. Notch lengths, *a*, are indicated above the image. TSA stress range and mean stress were 35 and 17.5 MPa, respectively. The multishade specimen images correspond to the dimensionless digital values of the TSA system while the plots represent the results of using Eq 3, i.e., SCF, vs. pixel position of a line scan between the two notch roots

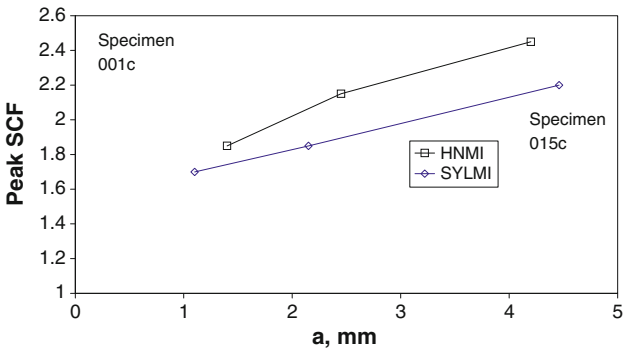

Fig. 4 Peak stress-concentration for 25.4-mm wide specimens with increasing notch length. TSA stress range and mean stress were 35 and 17.5 MPa, respectively

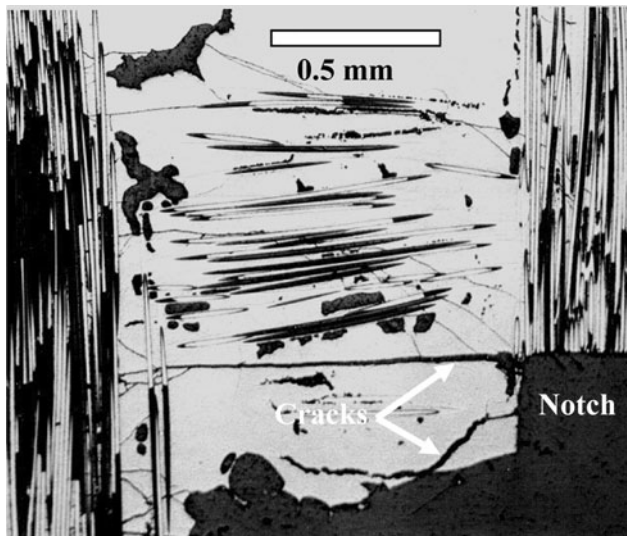

Fig. 5 Cracks emanating from notch for a fractured HNMI composite

SCF near the notch tip increased with increasing notch length for both composite systems. This behavior was expected and has been documented for other ceramic composites as well (Ref 10, 11).

Next, TSA data were collected at various points during load/unload/reload damage-inducing tensile tests (see Table 2 for test details). From acoustic emission data and destructive sectioning (see Fig. 5 and Ref 11), it was known that significant matrix cracking had occurred at the notch roots. The TSA readings were taken at near zero stress after unloading (TSA stress range of 0-35 MPa). Surprisingly, very little if any relief in the peak SCF at the notch tip was observed for either composite as summarized in Fig. 6. This lack of apparent stress-relief was similar to what was observed for a Nicalon™ fiber reinforced CVI SiC matrix composite in Ref 6. In that study, the peak stress-concentration at the notch tip was only reduced by about 8% after loading to 160 MPa compared with a Nicalon™ reinforced calcium aluminosilicate glass ceramic matrix where the stress-concentration was reduced by 26% after loading to 90 MPa. More specifically, the results in Ref 6 showed that one notch (representing the peak SCF) had an 8%

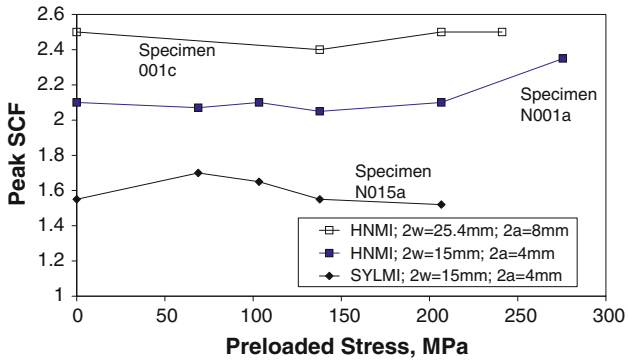

Fig. 6 The peak stress-concentration at the notch roots measured for three composite specimens after preloading to multiple, increasing stress levels as detailed in Table 2. TSA measurements were made after unloading from the maximum preloaded stress. TSA stress range and mean stress were 35 and 17.5 MPa, respectively

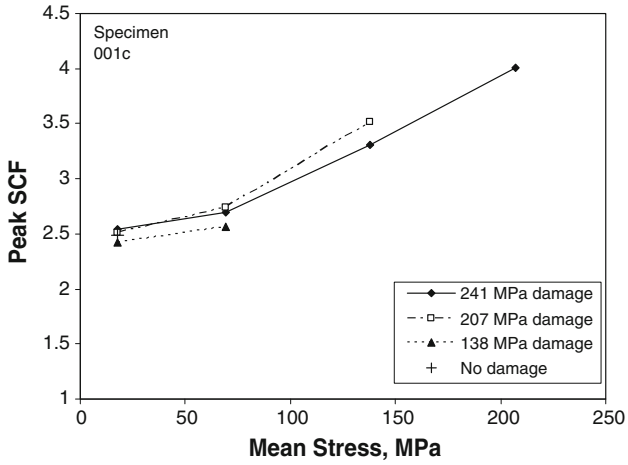

Fig. 7 Peak stress-concentration as a function of both damage state and mean stress during TSA measurements of a HNMI specimen. Each line represents a constant damage state defined by the maximum stress achieved prior to unloading. TSA stress range was 35 MPa while the mean stress was varied between 17.5 and 207 MPa

reduction while the second notch actually showed a SCF increase of 7%.

Lastly, the mean stress dependence of the peak SCF was studied concerning the HNMI composite. After each of the damage-inducing tensile tests, TSA measurements were made at multiple mean loads. The stress range during the TSA measurements was always maintained at 35 MPa while the mean stress was varied. Figure 7 summarizes the mean stress results concerning the peak SCF for the HNMI composite with various levels of damage. The figure shows a definite mean stress dependence concerning the peak SCF. With increasing mean stress, the specimen indicated an increasing peak SCF. Also noted was a bi-linear behavior indicated by the increased slope above the mean stress of 69 MPa. Figure 8 shows the TSA images at various mean stresses for the 241 MPa damage level. From Fig. 8, it was apparent that stress redistribution occurred. As a result, the left notch carried a bigger burden as the stress was increased, while the right notch indicated a slight decrease in the SCF with increasing mean stress.

3.2 Discussion

The two results that require further attention are the lack of apparent stress redistribution due to damage, and the issue of mean stress dependence concerning the SCF. First, focusing on the lack of observable stress redistribution, a strong notch-dependent behavior concerning the ultimate strength should exist for a material that lacks a mechanism for diffusing stresses in the vicinity of a notch. Strength results for both of these composites showed them to be only mildly notch sensitive (Ref 10, 11). In addition, acoustic emissions and post-test sectioning indicated substantial matrix cracking near the notch (≈4 cracks/mm for the HNMI composite). A possible explanation focused on stress redistribution in the form of intact fiber bundles near the notch tips taking on larger portions of the load as the adjacent matrix damage accumulated. Furthermore, the peak SCF data, plotted in Fig. 6, were probably related to particular fiber bundles within the surface plies adjacent to the notches. Although it was shown that the SCF values increased with damage, the effect on actual failure strengths was minimal since the elevated stresses were highly localized to the given fiber bundles. The reader should be aware that the TSA images had a pixel resolution of 0.25 mm^2 while the width of a typical fiber bundle was on the order of 1.2 mm (the matrix crack spacing in the vicinity of the notch was approximately 0.25 mm for the case of the HNMI composite). As a result, it is apparent that camera resolution was not an issue when describing the stress-state in an individual fiber bundle.

The mean stress dependence of the SCF data concerning the HNMI composite was probably related to the existence of compressive residual stresses in the matrix. These materials are known to exhibit stiffening upon unloading, presumably due to the closure of cracks at low stresses (Ref 11, 15-18). Figure 9 shows the hysteretic response of an unnotched, HNMI composite. Also indicated in the figure are values for the tangent modulus measured at initial unloading and initial reloading (Ref 18). Note the small drop in modulus for the unloading measurements as compared to the reloading values. The "true" elastic modulus (response) that was influenced by the matrix cracking in the material should correspond to the unloading modulus. When collecting TSA data with a mean stress close to zero (as indicated in Fig. 9), it was assumed that some of the matrix damage was masked by crack closure. With increasing mean stress, the matrix cracks were opened and the adjacent fiber bundles appeared to take on more of the load (see the TSA results in Fig. 7 and 8). The inflection point of the bilinear behavior in Fig. 7 may even relate to a critical stress that defines crack opening (i.e., the residual stress in the matrix). Note that a cautious approach is recommended in the interpretation of the TSA data related to these ceramic composites since it was focused on localized stresses within the surface plies of these rather complex material systems.

3.3 Adiabatic Assumption

After the above analyses, questions arose regarding the load frequency during TSA measurements and whether or not true adiabatic conditions were met at 10 Hz (selected due to the positive results attained in Ref 6 and the uniform phase images

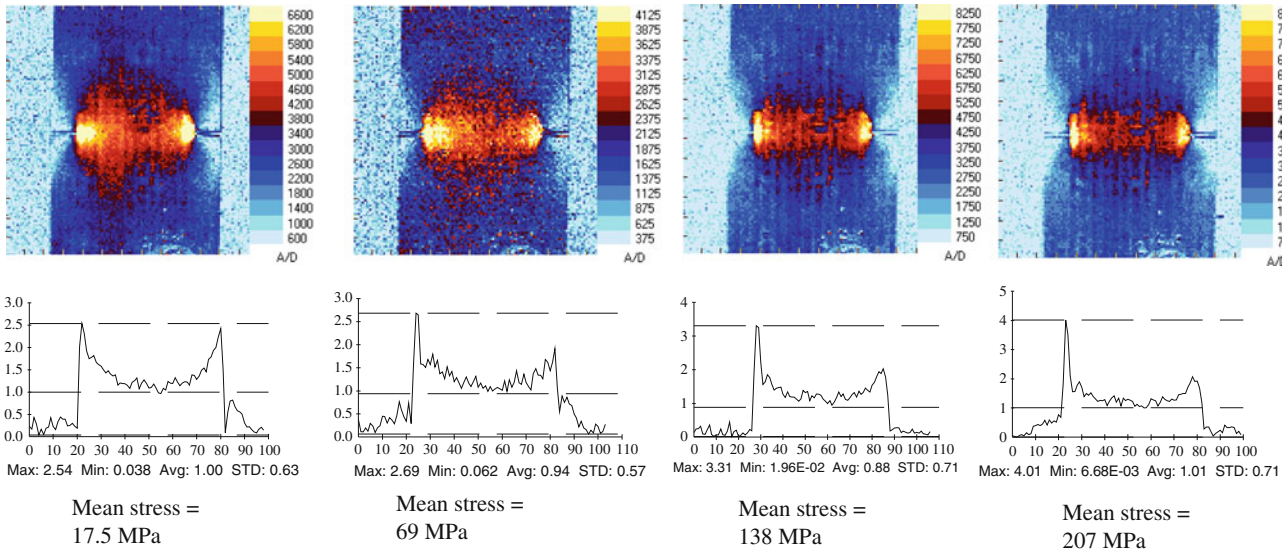

Fig. 8 TSA images of various mean stress values for the HNMI composite (specimen 001c). Each image has the same damage level defined as 241 MPa, the peak stress achieved during the load/unload tensile test. Note that the left notch length = 4.14 mm, and the right notch length = 4.27 mm. TSA stress range was 35 MPa with mean stresses between 17.5 and 207 MPa. The multishade specimen images correspond to the dimensionless digital values of the TSA system while the plots represent the results of using Eq 3, i.e., SCF, vs. pixel position of a line scan between the two notch roots

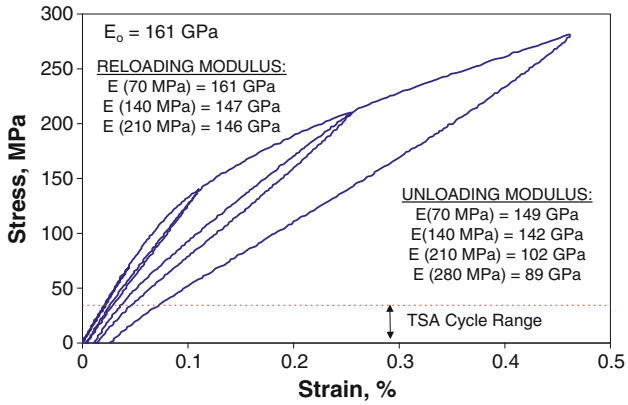

Fig. 9 Load/unload tensile stress-strain curve for an unnotched HNMI specimen showing the TSA cycle range and unloading and reloading moduli measured for each hysteresis loop. The effect of crack closure and apparent residual stress in the matrix is even greater for SYLMI

seen here). As a result further tests were conducted with the one remaining, HNMI double notch specimen (2.29 mm per notch). TSA data were collected with load frequencies of 3, 5, 10, 20, and 30 Hz (cyclic stress range of 0-34 MPa with mean stress of 17.5 MPa: three to six repetitions per test condition) in order to observe the thermal response in the high-stress region of the notch. It was understood that if the frequency was too low and an adiabatic condition was not achieved then there would be some conduction of heat away from highly stressed regions. Hence, the TSA observed stress-concentration under nonadiabatic conditions would be lower than the true value.

Figure 10 shows the typical results of these additional tests in the form of raw TSA images and the associated line scans between the two notches. It was apparent from the line scans that consistent adiabatic conditions were not met until 20 Hz. For the frequencies lower than 20 Hz, the peak stresses at the notch roots were attenuated, especially when observing the right notch. Figure 11 shows the SCF of the right notch as a function of frequency, again, indicating adiabatic conditions at 20 Hz and higher. These results do not negate the outcomes and discussions within this paper, but it should be realized that the observed/discussed SCFs may be a bit lower than SCFs attained under true adiabatic conditions (approximately 14% lower than the actual based on Fig. 11). Lastly, because of the complexity of these materials, creating a model in order to correct the nonadiabatic data is beyond the scope of the current paper, although, it may be of interest for a future study.

4. Conclusions

In this study, the stress fields adjacent to machined notch roots were examined for woven SiC fiber reinforced, melt-infiltrated SiC matrix composites with a BN interphase, utilizing either Hi-Nicalon™ fibers or the stiffer Sylramic® fibers. The SCF at the notch roots were obtained using the TSA technique. The SCF behavior was analyzed concerning notch length, damage level, and mean stress. It was shown that the peak SCF values for both composite systems increased with escalating notch lengths, as expected. Next, the peak SCF values were shown to increase with accumulated damage, again, for both composite types. This was assumed to be indicative of load redistribution from the damaged matrix to the intact fiber bundles adjacent to the notches. Lastly, the mean stress dependence of the SCF was addressed concerning the Hi-Nicalon composite. It was shown that SCF values increased with increasing mean stress. This behavior was assumed to

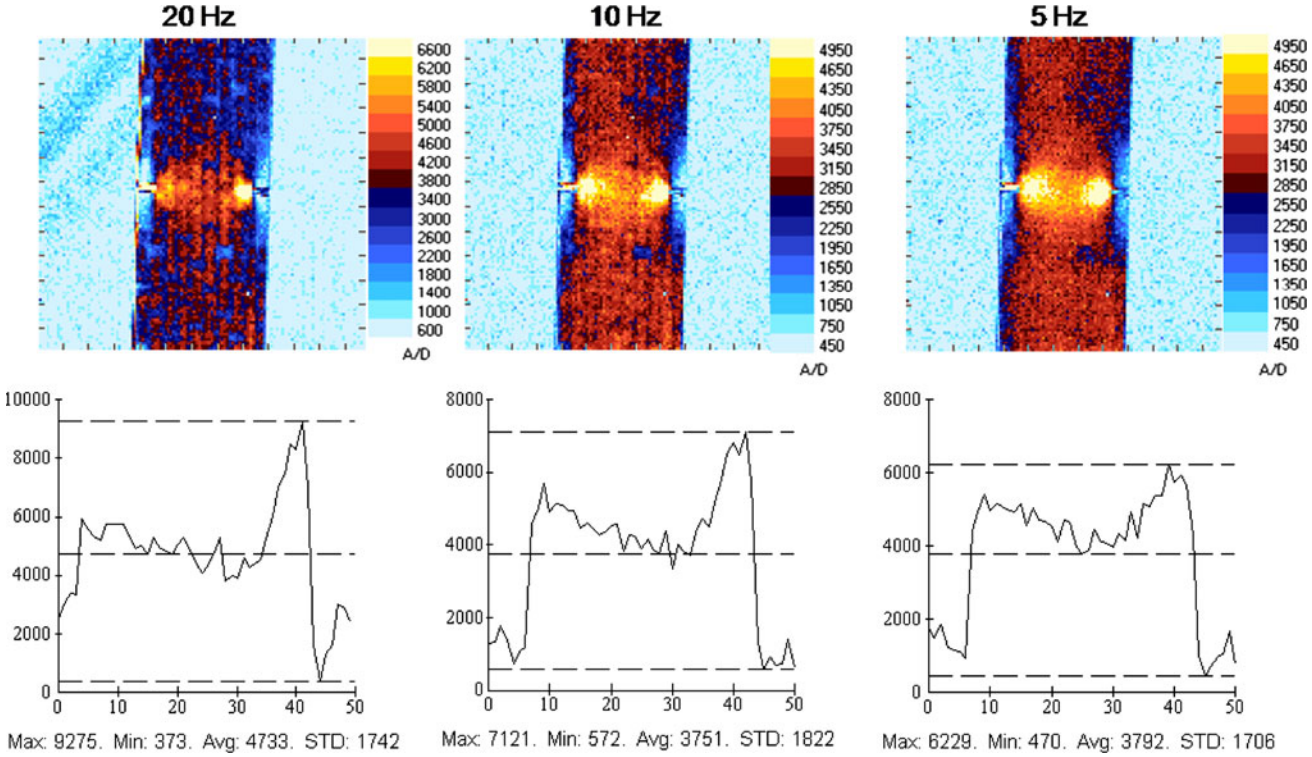

Fig. 10 TSA images and line scans between notches for HNMI (specimen 001) as a function of cyclic load frequency. Frequencies are indicated above the image. TSA stress range was 0-35 MPa (mean load was 17.5 MPa). The multishade specimen images correspond to the dimensionless digital values of the TSA system while the plots represent the results of using Eq 3, i.e., SCF, vs. pixel position of a line scan between the two notch roots

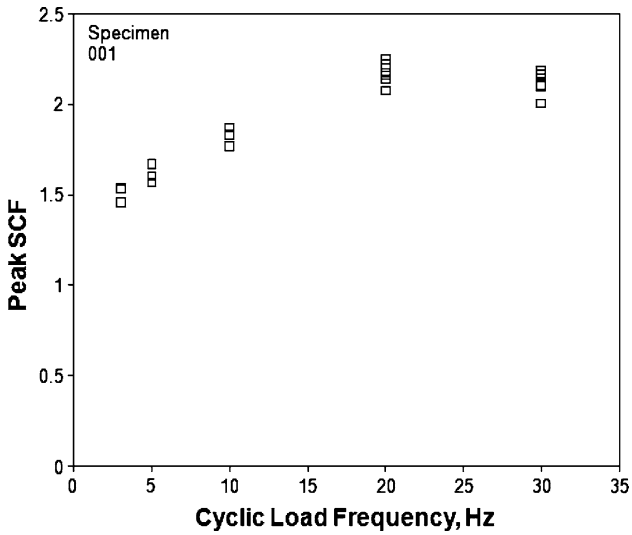

Fig. 11 Peak SCF (right notch) as a function of load frequency during TSA measurements

result from compressive residual stresses within the matrix material that cause crack closure at near zero stress levels. With increasing mean stress, the cracks opened and caused a redistribution of load onto the intact fiber bundles.

Acknowledgments

The authors would like to acknowledge Dr. George Baaklini and Dr. John Lekki of the NASA Glenn Research Center as well as the Integrated Vehicle Health Management Project within the Aviation Safety Program for providing the funding for this study.

References

1. D. Brewer, HSR/EPM Combustor Materials Development Program, *Mater. Sci. Eng.*, 1999, **A261**, p 284–291
2. C.M. Grondahl and T. Tsuchiya, "Performance Benefit Assessment of Ceramic Components in an MS9001FA Gas Turbine," 98-GT-186, 1998
3. A.J. Dean, G.S. Gorman, B. Bagepalli, K.L. Luthra, P.S. DiMascio, and R.M. Orenstein, "Design and Testing of CFCC Shroud and Combustor Components," 99-GT-235, 1999
4. T. Kameda, Y. Itoh, T. Hijikata, and T. Okamura, "Development of Continuous Fiber Reinforced Reaction Sintered Silicon Carbide Matrix Composite For Gas Turbine Hot Parts Application," 2000-GT00-67, 2000
5. A.G. Evans and F.W. Zok, The Mechanical Performance of Ceramic-Matrix Composites, *J. Mater. Sci.*, 1994, **29**, p 3857–3896
6. T.J. Mackin, T.E. Purcell, M.Y. He, and A.G. Evans, Notch Sensitivity and Stress Redistribution in Three Ceramic-Matrix Composites, *J. Am. Ceram. Soc.*, 1995, **78**, p 1719–1728
7. C. Cady, T.J. Mackin, and A.G. Evans, Silicon Carbide/Calcium Aluminosilicate: A Notch-Insensitive Ceramic-Matrix Composite, *J. Am. Ceram. Soc.*, 1995, **78**, p 77–82

8. R. John, D.J. Buchanan, and L.P. Zawada, *Notch-Sensitivity of a Woven Oxide/Oxide Ceramic Matrix Composite*, M.G. Jenkins et al., Ed., American Society for Testing and Materials, ASTM STP 1392, West Conshohocken, PA, 2000, p 172–185
9. C.G. Levi, J.Y. Yang, B.J. Dalgeish, F.W. Zok, and A.G. Evans, Processing and Performance of an All-Oxide Ceramic Composite, *J. Am. Ceram. Soc.*, 1998, **8**(1), p 2077–2086
10. J.C. McNulty, F.W. Zok, G.M. Genin, and A.G. Evans, Notch-Sensitivity of Fiber-Reinforced Ceramic-Matrix Composites: Effects of Inelastic Straining and Volume-Dependent Strength, *J. Am. Ceram. Soc.*, 1999, **82**, p 1217–1228
11. G.N. Morscher, J.Z. Gyekenyesi, and A.L. Gyekenyesi, Mechanical Behavior of Notched SiC/SiC Composites, *ASME International Gas Turbine and Aeroengine Congress*, no. 2001-GT-461, June 4–7, 2001
12. T.J. Mackin and M.C. Roberts, Thermoelastic Evaluation of Damage Evolution in Ceramic Matrix Composites: A Non-Contacting Stress Mapping Methodology, *J. Am. Ceram. Soc.*, 2000, **83**, p 337–343
13. W. Thomson (Lord Kelvin), On the Dynamical Theory of Heat, *Trans. Roy. Soc. Edinburgh*, 1853, **20**, p 261–283
14. J.R. Lesniak and B.R. Boyce, Differential Thermography Applied to Structural Integrity Assessment, *Proceedings of the International Conference on Thermal Sensing and Imaging Diagnostic Applications*, Orlando, FL, 2473, April 19-21, 1995
15. G.N. Morscher, R. Bhatt, and J.Z. Gyekenyesi, *Damage Accumulation in 2-D Woven SiC/SiC Ceramic Matrix Composites*, M.G. Jenkins et al., Ed., American Society for Testing and Materials, ASTM STP 1392, West Conshohocken, PA, 2000, p 306–319
16. J.C. McNulty and F.W. Zok, Application of Weakest-Link Fracture Statistics to Fiber-Reinforced Ceramic Matrix Composites, *J. Am. Ceram. Soc.*, 1997, **80**, p 1535–1543
17. M. Steen and J.L. Valles, *Unloading-Reloading Sequences and the Analysis of Mechanical Test Results for Continuous Fiber Ceramic Composites*, M.G. Jenkins et al., Ed., American Society for Testing and Materials, ASTM STP 1309, West Conshohocken, PA, 1997, p 49–65
18. J.M. Domergue, E. Vagaggini, and A.G. Evans, Relationships Between Hysteresis Measurements and the Constituent Properties of Ceramic Matrix Composites: II. Experimental Studies on Unidirectional Materials, *J. Am. Ceram. Soc.*, 1995, **78**, p 2721–2723